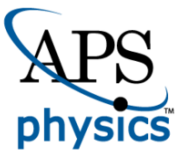

Quadrupolar Exchange-Only Spin Qubit

Maximilian Russ, J. R. Petta, and Guido Burkard

Phys. Rev. Lett. **121**, 177701 — Published 25 October 2018

DOI: 10.1103/PhysRevLett.121.177701

A quadrupolar exchange-only spin qubit

Maximilian Russ,[1] J. R. Petta,[2] and Guido Burkard[1]

[1] *Department of Physics, University of Konstanz, D-78457 Konstanz, Germany*
[2] *Department of Physics, Princeton University, Princeton, New Jersey 08544, USA*

We propose a quadrupolar exchange-only spin (QUEX) qubit that is highly robust against charge noise and nuclear spin dephasing, the dominant decoherence mechanisms in quantum dots. The qubit consists of four electrons trapped in three quantum dots, and operates in a decoherence-free subspace to mitigate dephasing due to nuclear spins. To reduce sensitivity to charge noise, the qubit can be completely operated at an extended charge noise sweet spot that is first-order insensitive to electrical fluctuations. Due to on-site exchange mediated by the Coulomb interaction, the qubit energy splitting is electrically controllable and can amount to several GHz even in the "off" configuration, making it compatible with conventional microwave cavities.

Introduction Electron spin qubits in semiconductor quantum dots have recently demonstrated their capability as components in a working quantum processor [1–4]. With simple quantum algorithms having now been demonstrated, there is a strong motivation for building a large-scale quantum computer using spin qubits due to their long intrinsic coherence times and fast gate operation times [5–8]. Spin qubits in silicon additionally benefit from state-of-the-art industrial nanofabrication techniques for scalability and the possibility of isotopic enrichment to increase coherence times. While there are many different implementations of spin qubits, the exchange-only qubit [9–15] is unique since it can be fully controlled using dc gate voltage pulses. The decoherence-free subspace encoding also makes exchange-only spin qubits insensitive to overall (long-wavelength) magnetic field fluctuations [9, 16, 17]. However, all experimental demonstrations until now suffer from decoherence due to charge noise and local (short-wavelength) magnetic field gradient (LMFG) noise, thus limiting the performance of the qubit [12–15, 18].

Protection against charge noise is provided by operating qubits at a so-called charge noise "sweet spot", a point of operation which is first-order insensitive to electric fluctuations [18–26]. However, the energy splitting at these sweet spots is too small to couple the qubit to conventional superconducting resonators required for long-distance entanglement protocols [22, 27–34]. Moreover, three-spin exchange-only qubits are sensitive to LMFG noise [26, 35–37], which can arise from fluctuating nuclear spins or Meissner expulsion of magnetic fields near superconducting gates. These gradients limit spin coherence times and can result in leakage, i.e., the loss of information into the non-computational subspace. Additionally, while a single exchange-only qubit or hybrid qubit is insensitive to fluctuations in the overall magnetic field, an array of exchange coupled exchange-only (hybrid) qubits does not benefit from this protection since each exchange-only qubit can acquire a slightly different phase.

In this Letter, we propose a quadrupolar exchange-only spin (QUEX) qubit that allows for universal quantum computation with high-speed qubit operations and very long coherence times. The QUEX qubit is operated in the 4 electron regime, with the 4 electrons distributed on 3 series-coupled semiconductor quantum dots [see Fig. 1(a)] and is encoded in the low-energy subspace with total spin $S = 0$. This encoding makes the QUEX qubit insensitive to overall (long-wavelength) magnetic fields, first-order insensitive to LMFG noise [16, 17, 38], and no global phases are acquired from long-range magnetic fields, thus there is no desynchronization problem if used in a large-scale array. Compared to the singlet-singlet qubit [38], the QUEX qubit offers a simplified architecture requiring only three dots and two detuning parameters. As with the exchange-only qubit [9], single-qubit operations in the QUEX qubit can be driven using either dc pulses or ac modulation. Compared to the exchange-only [9–14, 18–23, 26, 39] and the hybrid [26, 40–44] qubit, the QUEX qubit offers an increased protection against charge noise [43, 45] due to an extended charge noise sweet spot. This arises from the addition of the fourth electron which flattens the energy bands and provides a qubit energy splitting at the sweet spot which is electrically controllable and can amount to several GHz

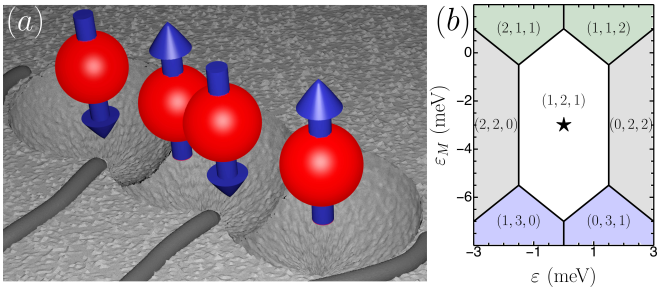

FIG. 1. (a) Illustration of a four-electron spin qubit residing in an electrostatically defined triple quantum dot (TQD). The four spins are coupled via inter-dot and onsite exchange interaction. The center dot is occupied by two electrons, giving rise to a large and electrostatically tunable energy splitting. (b) TQD charge stability diagram as a function of ε and ε_M. The optimal operating point is marked by the star.

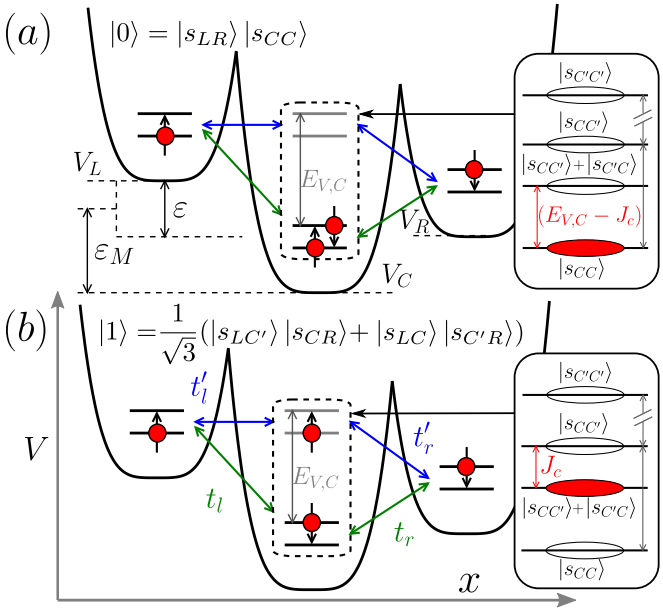

FIG. 2. Qubit basis states and TQD confining potential $V(x)$. The left and right dots each contain one electron in the ground state (black level). The middle dot contains two electrons, one of which can occupy an excited valley state (grey level), lying $E_{V,C}$ above the ground state. The electrons are allowed to hop with valley conserving (green $t_{l,r}$), and valley non-conserving (blue $t'_{l,r}$) tunneling. (a) Possible spin configuration of the qubit state $|0\rangle$. (Inset) Spin configuration in the center dot. Both electrons reside in the valley ground state. (b) Possible spin configuration of the qubit state $|1\rangle$. (Inset) Spin configuration in the center dot. One electron resides in the valley ground state while the second electron occupies an excited valley state.

even in the "off" configuration, thus, making it compatible with conventional superconducting resonators. Building on recent experiments showing that strong coupling of semiconductor qubits [15, 46–50] to electromagnetic resonators is feasible, we present an electrically switchable two-qubit interaction [34] making use of the large and strongly tunable qubit splitting.

Qubit design A defining feature of the QUEX qubit is its use of the valley degree of freedom in Si to achieve an energy splitting that is compatible with conventional superconducting cavities with $4-10\,$GHz resonance frequencies. The QUEX qubit is implemented in a TQD that contains a total of four electrons in the (1,2,1) charge configuration [see Figs. 1 and 2(a)]. Here (N_L, N_C, N_R) denote the number of electrons confined in each of the three dots. For later convenience we define the dipolar detuning $\varepsilon \equiv (V_L - V_R)/2$ and the quadrupolar detuning $\varepsilon_M \equiv V_C - (V_L + V_R)/2$ [see Fig. 2 (a)].

Silicon quantum dots typically have relatively large orbital energies $E_{\rm orb} = 3-5\,$meV [51, 52]. In contrast, the smaller valley splittings $E_{V,C} = 20-250\,\mu$eV are compatible with microwave frequency photons (1 GHz $\sim 4.2\,\mu$eV) [51, 53]. In the QUEX qubit, the valley degree of freedom plays a crucial role in the middle dot, as it adds a level that can be treated as an additional fourth pseudo-dot. An external (homogeneous) magnetic field with Zeeman splitting $E_Z \ll E_{V,C} \ll E_{\rm orb}$ energetically separates states according to S_z. The QUEX qubit resides in the two lowest energy levels in the $S = S_z = 0$ subspace with the two following logical spin qubit states [38, 54]

$$|0\rangle = |s_{LR}\rangle\,|s_{CC}\rangle \tag{1}$$

$$|1\rangle = \frac{1}{\sqrt{3}}(|s_{LC'}\rangle\,|s_{CR}\rangle + |s_{LC}\rangle\,|s_{C'R}\rangle). \tag{2}$$

Here, $|s_{\mu\nu}\rangle$ denotes the singlet state formed by two electrons in orbitals μ and ν with $\mu,\nu = L, C, C', R$ where L (R) reside in the left QD (right QD) and $C, (C')$ reside in the lower (upper) valley in the center QD. Note that both qubit states are constructed using only two-electron singlet states making them resilient to LMFG.

We describe the dynamics of the QUEX qubit by the following effective Hamiltonian

$$H = J_0\,|0\rangle\langle 0| + (J_1 + E_{V,C} - J_C)\,|1\rangle\langle 1| + J_x\sigma_+ + J_x^*\sigma_-, \tag{3}$$

with the qubit raising and lowering operator $\sigma_+ = |0\rangle\langle 1|$ and $\sigma_- = \sigma_+^\dagger = |1\rangle\langle 0|$. Here, J_0 and J_1 are real-valued and J_x complex-valued exchange couplings from virtual tunneling processes to states with a (2,2,0), (2,1,1), (1,3,0), (0,3,1), (1,1,2) and (0,2,2) charge configuration, $E_{V,C}$ is the valley splitting in the center QD, and J_C is the onsite Coulomb-exchange coupling between the electrons occupying the center QD. The phase of J_x depends on the phase an electron acquires by consecutively tunneling from the lower to the excited valley state on the center dot via an intermediate state on the left or right dot (see Fig. 2). For later convenience, we can also write $J_\mu = \sum_\nu J_\mu^\nu$ with $\mu = 0, 1, x$ and $\nu = l, l', r, r'$ where J_μ^l (J_μ^L) denotes exchange coupling via valley conserving (non-conserving) tunneling of an electron from the center QD to the left QD and similarly for J_μ^r (J_μ^R) to the right QD. The qubit splitting for $|J_x| \ll |E_{V,C} - J_C|$ is given by

$$\omega_q \approx (J_1 + E_{V,C} - J_C - J_0) + \frac{|J_x|^2}{2(J_1 + E_{V,C} - J_C - J_0)}. \tag{4}$$

The explicit expressions for the exchange parameters and a detailed derivation of the effective Hamiltonian (3) can be found in [55].

Initialization and Readout Figures 3(a)-(b) illustrate the initialization protocol. To prepare the system in state $|\text{init}\rangle = |s_{LL}\rangle\,|s_{RR}\rangle$ the detuning parameter ε_M is set such that the (2,0,2) charge configuration is the ground state [Fig. 3 (a)]. Due to the large single dot exchange splittings, the two electron ground state in the left and

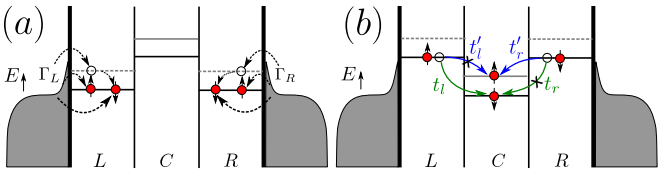

FIG. 3. Protocol for initializing the QUEX qubit: First the (2,0,2) charge configuration regime (a) is prepared by loading the left and right QD with two electrons in the spin-up and spin-down state of the lowest valley. (b) Adiabatic tuning from the (2,0,2) to the (1,2,1) charge state directly maps $|\text{init}\rangle \rightarrow |1\rangle$. Readout is performed by reversing the initialization sequence, as described in the main text.

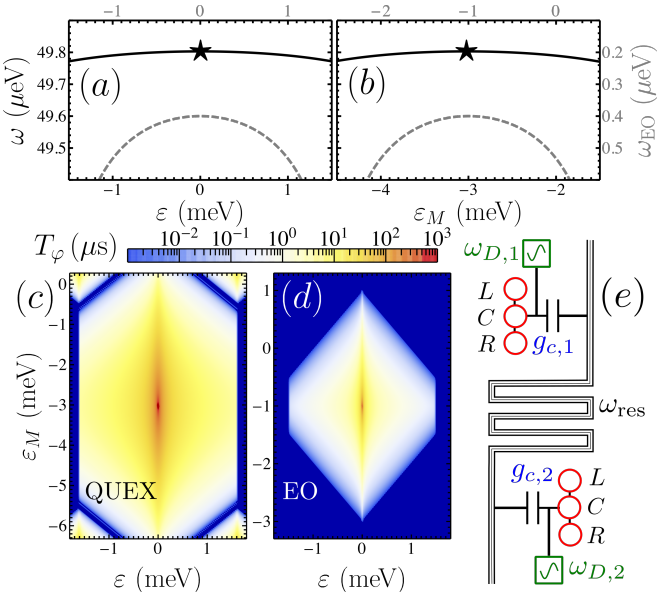

FIG. 4. Qubit energy splitting ω as a function of (a) the dipolar detuning ε and (b) quadrupolar detuning ε_M. The stars in (a) and (b) mark the sweet spots where $\partial\omega_q/\partial\varepsilon = 0$ and $\partial\omega_q/\partial\varepsilon_M = 0$. For comparison the energy gap ω_{EO} of the conventional exchange-only qubit (gray dashed lines) is shown with identical parameter settings. The curvature of ω_{EO} is larger in magnitude causing a higher susceptibility to charge noise. (c) Qubit dephasing time T_φ due to charge fluctuations as a function of ε and ε_M for $t_l' = t_r'$ using realistic parameters [55]. The calculations shows that $T_\varphi > 100\,\mu$s if the qubit is operated at the charge noise sweet spot. (d) Qubit dephasing time for the conventional exchange-only (EO) qubit with identical parameter settings. Expressions for the calculation of T_φ can be found in Refs. [21, 22]. (e) Schematic of the microwave resonator mediated two-qubit coupling. A cavity with resonance frequency ω_{res} is coupled to the center dot with an effective charge-cavity coupling rate $g_{c,i}$. Each qubit is simultaneously driven at a frequency $\omega_{D,i}$.

right dots is a singlet [56] and can be prepared with high fidelity [57]. Adiabatic tuning of ε_M into a configuration where the (1,2,1) charge configuration is the ground state [Fig. 3(b)] maps $|\text{init}\rangle \rightarrow |1\rangle$ through spin conserving tunneling events. Readout is performed in reverse, i.e., by detecting the tunneling of the electrons from the center dot to the left and right dots. Tunneling of $|1\rangle$ to the (2,0,2) ground state is allowed, but tunneling of $|0\rangle$ to the (2,0,2) ground state is Pauli blocked, similar to singlet-triplet readout in double dots [56]. Charge detection therefore provides a fast and high fidelity readout scheme.

Decoherence properties The Si/SiO$_x$ and Si/SiGe systems appear to be most favorable for the experimental realization of the QUEX qubit due to their large, and somewhat tunable, valley splitting. Since the four spin encoding of the QUEX is resilient to fluctuating LMFG noise [38] an implementation in natural silicon is still possible without significantly decreasing the decoherence time. Note that this protection against fluctuating LMFG arises solely from the singlet-singlet encoding of the qubit basis states and is independent of the spatial wavefunctions of these states [38]. The QUEX qubit possesses a full charge noise sweet spot where the qubit is first order insensitive to charge fluctuations in both detuning parameters $\varepsilon, \varepsilon_M$ [see Figs. 4 (a)-(b)]. From the condition $\partial_\varepsilon\omega_q = \partial_{\varepsilon_M}\omega_q = 0$ and assuming $|t_l| = |t_l'|$, $|t_r| = |t_r'|$, and symmetric charging energies U, we find a double sweet spot at $\varepsilon = 0$ and $\varepsilon_M = (J_c - E_{V,C})/2 - U$. Arbitrary non-equal charging energies only lead to a shift of the sweet spot in detuning space [55]. Importantly, the sweet spot of the QUEX qubit is very flat compared to the conventional exchange-only qubit, i.e., the curvature of $\omega(\varepsilon, \varepsilon_M)$ is reduced by a factor $(U - U_n)/(U + U_n)$ with the onsite- and cross-(nearest-neighbor)-charging energy U and U_n, therefore protecting it significantly better against charge noise. A related increase in protection is observed when using the center dot as a remote coupler between two spins in the left and right dot due to the screening from the doubly occupied dot [58]. Numerical simulations that take into account the dominant charge fluctuations in Si are shown in Fig. 4 (c). We predict dephasing times T_φ on the order of several hundreds of microseconds for the QUEX qubit assuming realistic parameters, one order of magnitude longer than for the conventional exchange-only qubit (Fig. 4 (d) and Refs. [22, 26]). A full study for the general case $t_l \neq t_l'$ and $t_r \neq t_r'$ yields qualitatively similar results [55]. Additional dephasing may arise from the electric field dependence of the valley splitting E_V in SiMOS devices. This contribution is negligible for Si/SiGe devices.

Single-qubit operations Arbitrary single-qubit gates can be implemented by pulsing the exchange interactions, J_μ^ν. Assuming valley-orbit conserving and non-conserving tunneling to be equal ($t_l = t_l'$ and $t_r = t_r'$),

the Hamiltonian (3) can be rewritten as

$$H_q = \frac{1}{8}(2J_0^l - 3J_1^l + 2J_0^r - 3J_1^r + 8E_{V,C} - 8J_C)\sigma_z + \frac{1}{4}\frac{\sqrt{3}}{\sqrt{8}}(J_0^l + J_1^l - J_0^r - J_1^r)\sigma_x. \quad (5)$$

Here, we introduced the Pauli operators $\sigma_z = |0\rangle\langle 0| - |1\rangle\langle 1|$ and $\sigma_x = \sigma_+ + \sigma_-$. Therefore, pulsing $J_q^l = J_q^r$ results in pure (and fast) z-rotations while pulses with $J_q^l \neq J_q^r$ yield rotations around a tilted axis [59]. Experimentally, the exchange interaction can either be controlled through detuning [56] or tunnel barrier control [18, 24, 25, 60]. Barrier control has the advantage that it operates the qubit at the charge noise sweet spot, thus, mitigating decoherence from charge noise during the exchange pulse. This statement, however, is only valid for $t_l \approx t_l'$ and $t_r \approx t_r'$ since otherwise the position of the sweet spot depends on the tunneling and moves during the qubit operation. In the latter case, one can combine barrier control with tilting control to compensate for the shift of the sweet spot. Similar pulsing schemes are commonly implemented to cancel crosstalk between electrostatic gates [61].

A more natural way of implementing single-qubit rotations in the QUEX qubit is to modulate the exchange coupling, $J_\mu^\nu \to J_\mu^\nu + j_\mu^\nu \cos(\omega_D + \phi)$ analogous to the resonant exchange (RX) qubit [12, 19, 26]. In a frame rotating with the drive frequency ω_D, and neglecting fast oscillations at $2\omega_D$, the Hamiltonian (3) can be written in its eigenbasis as

$$H_q = \frac{1}{2}(\omega_q - \omega_D)\sigma_z + \frac{J_x^1}{2}\left(e^{i\phi}|1\rangle\langle 0| + e^{-i\phi}|0\rangle\langle 1|\right). \quad (6)$$

Here, the drive amplitude $J_x^1 = A_q j_x \big[J_x \partial(J_1 - J_0)/\partial q - (J_1 - J_0)\partial J_x/\partial q\big]/(2\omega_q)$ sets the Rabi flip time $\tau_x^{-1} \propto A_q \propto J_x^1$, where A_q denotes the amplitude of the driving of the parameter $q \in \{\varepsilon, \varepsilon_M, t_{l,r}, t_{l,r}'\}$. The phase ϕ can be used to adjust the qubit rotation axis. Experimentally, this can realized by parametric modulation of either the detuning parameters, $\varepsilon, \varepsilon_M$, or the tunneling couplings, $t_{l,r}$ and $t_{l,r}'$. Using realistic parameters we find $A_{\varepsilon_M} \approx 0.13\,\mu$eV, thus, $\tau_x = 30$ ns while driving at the charge noise double sweet spot [55]. Modulation of the tunnel barrier has the additional benefit of providing a dynamic sweet spot, where the Rabi drive is first-order insensitive to fluctuations in detuning, $\partial J_x^1/\partial q = 0$. Recent experiments show that charge noise affecting the Rabi frequency significantly reduces the number of coherent exchange oscillations [18]. Thanks to the naturally large energy splitting of the qubit ω_q counter-rotating terms are small and off-resonant transitions are strongly suppressed, making strong driving feasible.

Two-qubit interaction Exchange-only qubits are limited to short-ranged, exchange-based operations requiring complex pulse sequences [9, 16, 17, 62, 63]. The QUEX qubit, with its large and tunable energy splitting, enables near-resonant coupling to high frequency resonators giving rise to new entanglement generation protocols [64]. We now describe a resonantly-driven, cavity-mediated two-qubit entanglement protocol [28, 31, 32, 34, 65].

For this setup a superconducting cavity with resonance frequency $\omega_{\rm res}$ is capacitively coupled to the electrostatic potential V_C at the center QD while V_C of each qubit is simultaneously modulated with frequency $\omega_D \approx \omega_q$ and phase ϕ [see Fig. 4 (e)]. Thus, $V_C \to V_C(t) = V_C^0 + V_C^1\cos(\omega_D + \phi) + g_c(a + a^\dagger)$. Here $a^\dagger$ (a) creates (annihilates) a cavity photon with frequency $\omega_{\rm res}$, and $g_c \propto \sqrt{Z}$ is the charge-photon coupling strength and Z is the characteristic impedance of the resonator [15, 48, 50, 66]. The effect of $V_C(t)$ on each qubit is described by the Hamiltonian [55]

$$H_{\rm int} = \omega_{\rm res} a^\dagger a + g\sigma_x(a + a^\dagger) + \Omega\cos(\omega_D + \phi)\sigma_x, \quad (7)$$

where the second term describes the qubit-cavity interaction with coupling strength $g = g_c\langle 0|\partial_{V_C} H_q(V_C)|1\rangle$ and the last term induces a spin-flip with Rabi frequency $\Omega = V_C^1\langle 0|\partial_{V_C} H_q(V_C)|1\rangle$. Following the protocol described in Ref. [34], Hamiltonian (7) generates "red" and "blue" sideband transitions for the particular choice of $\Omega = \pm(\omega_{\rm res} - \omega_D)$ and $\omega_D = \omega_q$

$$H_\mp(g, \phi) = \frac{g}{2}\left(e^{\pm i\phi} a^\dagger \sigma_\mp + e^{\mp i\phi} a \sigma_\pm\right). \quad (8)$$

An entangling controlled-Z (CZ) gate is constructed using pulses of "red" and "blue" sideband transition gates $S_\mp(\phi, \tau) \equiv \exp[-itH_\mp(g, \phi)]$ combined with single-qubit rotations [34]. Using experimentally feasible parameter settings, a CZ gate is possible within $\tau \approx 340$ ns [55]. For this implementation it is essential to be able to tune the qubit near resonance to fulfill $\Omega = \pm(\omega_{\rm res} - \omega_D)$ while simultaneously matching $\omega_D = \omega_q$, therefore, requiring a large and controllable qubit splitting. Alternative two-qubit coupling schemes include exchange-based interaction [62, 63] and capacitative coupling [41, 67].

Discussion In summary, we have proposed a quadrupolar exchange (QUEX) spin qubit that uses the spin of four electrons in a TQD and gives rise to a large controllable qubit splitting. The decoherence-free ($S = 0$) qubit encoding makes the qubit insensitive to local magnetic field gradients primarily from nuclear spins and Meissner expulsion. Further the large energy gap and flat qubit dispersion suppresses the susceptibility to charge noise and the qubit can be fully operated at a (extended) charge noise sweet spot. We predict dephasing times exceeding $\sim 100\,\mu$s at the sweet spot, one order of magnitude longer than for the conventional exchange-only qubit, allowing for a high quality qubit implementation. A symmetric readout and initialization protocol can be used to perform fast and high fidelity measurements. Together with the proposed cavity-mediated,

long-distance entangling protocol, these properties render the QUEX qubit suitable for implementation in a large-scale quantum information processing architecture.

We acknowledge funding from ARO through Grant No. W911NF-15-1-0149 and the DFG through SFB 767. We thank M. Benito and J.M. Taylor for helpful discussions.

[1] M. Veldhorst, C. H. Yang, J. C. C. Hwang, W. Huang, J. P. Dehollain, J. T. Muhonen, S. Simmons, A. Laucht, F. E. Hudson, K. M. Itoh, A. Morello, and A. S. Dzurak, Nature (London) **526**, 410 (2015).

[2] J. Yoneda, K. Takeda, T. Otsuka, T. Nakajima, M. R. Delbecq, G. Allison, T. Honda, T. Kodera, S. Oda, Y. Hoshi, N. Usami, K. M. Itoh, and S. Tarucha, Nat. Nanotechnol. **13**, 102 (2018).

[3] D. M. Zajac, A. J. Sigillito, M. Russ, F. Borjans, J. M. Taylor, G. Burkard, and J. R. Petta, Science **359**, 439 (2018).

[4] T. F. Watson, S. G. J. Philips, E. Kawakami, D. R. Ward, P. Scarlino, M. Veldhorst, D. E. Savage, M. G. Lagally, M. Friesen, S. N. Coppersmith, M. A. Eriksson, and L. M. K. Vandersypen, Nature (London) **555**, 633 (2018).

[5] D. Loss and D. P. DiVincenzo, Phys. Rev. A **57**, 120 (1998).

[6] R. Hanson, L. P. Kouwenhoven, J. R. Petta, S. Tarucha, and L. M. K. Vandersypen, Rev. Mod. Phys. **79**, 1217 (2007).

[7] C. Kloeffel and D. Loss, Annu. Rev. Condens. Matter Phys. **4**, 51 (2013).

[8] F. A. Zwanenburg, A. S. Dzurak, A. Morello, M. Y. Simmons, L. C. L. Hollenberg, G. Klimeck, S. Rogge, S. N. Coppersmith, and M. A. Eriksson, Rev. Mod. Phys. **85**, 961 (2013).

[9] D. P. DiVincenzo, D. Bacon, J. Kempe, G. Burkard, and K. B. Whaley, Nature (London) **408**, 339 (2000).

[10] E. A. Laird, J. M. Taylor, D. P. DiVincenzo, C. M. Marcus, M. P. Hanson, and A. C. Gossard, Phys. Rev. B **82**, 075403 (2010).

[11] L. Gaudreau, G. Granger, A. Kam, G. C. Aers, S. A. Studenikin, P. Zawadzki, M. Pioro-Ladriere, Z. R. Wasilewski, and A. S. Sachrajda, Nat. Phys. **8**, 54 (2012).

[12] J. Medford, J. Beil, J. M. Taylor, E. I. Rashba, H. Lu, A. C. Gossard, and C. M. Marcus, Phys. Rev. Lett. **111**, 050501 (2013).

[13] J. Medford, J. Beil, J. M. Taylor, S. D. Bartlett, A. C. Doherty, E. I. Rashba, D. P. DiVincenzo, H. Lu, A. C. Gossard, and C. M. Marcus, Nat. Nanotechnol. **8**, 654 (2013).

[14] K. Eng, T. D. Ladd, A. Smith, M. G. Borselli, A. A. Kiselev, B. H. Fong, K. S. Holabird, T. M. Hazard, B. Huang, P. W. Deelman, I. Milosavljevic, A. E. Schmitz, R. S. Ross, M. F. Gyure, and A. T. Hunter, Sci. Adv. **1**, e1500214 (2015).

[15] A. J. Landig, J. V. Koski, P. Scarlino, U. C. Mendes, A. Blais, C. Reichl, W. Wegscheider, A. Wallraff, K. Ensslin, and T. Ihn, Nature **560**, 179 (2018).

[16] D. Bacon, J. Kempe, D. A. Lidar, and K. B. Whaley, Phys. Rev. Lett. **85**, 1758 (2000).

[17] J. Kempe, D. Bacon, D. A. Lidar, and K. B. Whaley, Phys. Rev. A **63**, 042307 (2001).

[18] F. K. Malinowski, F. Martins, P. D. Nissen, S. Fallahi, G. C. Gardner, M. J. Manfra, C. M. Marcus, and F. Kuemmeth, Phys. Rev. B **96**, 045443 (2017).

[19] J. M. Taylor, V. Srinivasa, and J. Medford, Phys. Rev. Lett. **111**, 050502 (2013).

[20] J. Fei, J.-T. Hung, T. S. Koh, Y.-P. Shim, S. N. Coppersmith, X. Hu, and M. Friesen, Phys. Rev. B **91**, 205434 (2015).

[21] M. Russ and G. Burkard, Phys. Rev. B **91**, 235411 (2015).

[22] M. Russ, F. Ginzel, and G. Burkard, Phys. Rev. B **94**, 165411 (2016).

[23] Y.-P. Shim and C. Tahan, Phys. Rev. B **93**, 121410 (2016).

[24] M. D. Reed, B. M. Maune, R. W. Andrews, M. G. Borselli, K. Eng, M. P. Jura, A. A. Kiselev, T. D. Ladd, S. T. Merkel, I. Milosavljevic, E. J. Pritchett, M. T. Rakher, R. S. Ross, A. E. Schmitz, A. Smith, J. A. Wright, M. F. Gyure, and A. T. Hunter, Phys. Rev. Lett. **116**, 110402 (2016).

[25] F. Martins, F. K. Malinowski, P. D. Nissen, E. Barnes, S. Fallahi, G. C. Gardner, M. J. Manfra, C. M. Marcus, and F. Kuemmeth, Phys. Rev. Lett. **116**, 116801 (2016).

[26] M. Russ and G. Burkard, J. Phys. Condens. Matter **29**, 393001 (2017).

[27] A. Imamoglu, D. D. Awschalom, G. Burkard, D. P. DiVincenzo, D. Loss, M. Sherwin, and A. Small, Phys. Rev. Lett. **83**, 4204 (1999).

[28] A. M. Childs and I. L. Chuang, Phys. Rev. A **63**, 012306 (2000).

[29] L. Childress, A. S. Sørensen, and M. D. Lukin, Phys. Rev. A **69**, 042302 (2004).

[30] G. Burkard and A. Imamoglu, Phys. Rev. B **74**, 041307 (2006).

[31] A. Wallraff, D. I. Schuster, A. Blais, J. M. Gambetta, J. Schreier, L. Frunzio, M. H. Devoret, S. M. Girvin, and R. J. Schoelkopf, Phys. Rev. Lett. **99**, 050501 (2007).

[32] P. J. Leek, S. Filipp, P. Maurer, M. Baur, R. Bianchetti, J. M. Fink, M. Göppl, L. Steffen, and A. Wallraff, Phys. Rev. B **79**, 180511 (2009).

[33] M. Russ and G. Burkard, Phys. Rev. B **92**, 205412 (2015).

[34] V. Srinivasa, J. M. Taylor, and C. Tahan, Phys. Rev. B **94**, 205421 (2016).

[35] J.-T. Hung, J. Fei, M. Friesen, and X. Hu, Phys. Rev. B **90**, 045308 (2014).

[36] S. Mehl, Phys. Rev. B **91**, 035430 (2015).

[37] C. G. Péterfalvi and G. Burkard, Phys. Rev. B **96**, 245412 (2017).

[38] A. Sala and J. Danon, Phys. Rev. B **95**, 241303 (2017).

[39] G. Poulin-Lamarre, J. Thorgrimson, S. A. Studenikin, G. C. Aers, A. Kam, P. Zawadzki, Z. R. Wasilewski, and A. S. Sachrajda, Phys. Rev. B **91**, 125417 (2015).

[40] Z. Shi, C. B. Simmons, J. R. Prance, J. K. Gamble, T. S. Koh, Y.-P. Shim, X. Hu, D. E. Savage, M. G. Lagally, M. A. Eriksson, M. Friesen, and S. N. Coppersmith, Phys. Rev. Lett. **108**, 140503 (2012).

[41] T. S. Koh, J. K. Gamble, M. Friesen, M. A. Eriksson, and S. N. Coppersmith, Phys. Rev. Lett. **109**, 250503 (2012).

[42] G. Cao, H.-O. Li, G.-D. Yu, B.-C. Wang, B.-B. Chen, X.-X. Song, M. Xiao, G.-C. Guo, H.-W. Jiang, X. Hu, and G.-P. Guo, Phys. Rev. Lett. **116**, 086801 (2016).

[43] B. Thorgrimsson, D. Kim, Y.-C. Yang, L. W. Smith,

C. B. Simmons, D. R. Ward, R. H. Foote, J. Corrigan, D. E. Savage, M. G. Lagally, M. Friesen, S. N. Coppersmith, and M. A. Eriksson, npj Quantum Inf. **3**, 32 (2017).
[44] B.-C. Wang, G. Cao, H.-O. Li, M. Xiao, G.-C. Guo, X. Hu, H.-W. Jiang, and G.-P. Guo, Phys. Rev. Applied **8**, 064035 (2017).
[45] X. Mi, S. Kohler, and J. R. Petta, 1805.04545v1.
[46] J. J. Viennot, M. R. Delbecq, L. E. Bruhat, M. C. Dartiailh, M. M. Desjardins, M. Baillergeau, A. Cottet, and T. Kontos, Comptes Rendus Physique **17**, 705 (2016).
[47] X. Mi, J. V. Cady, D. M. Zajac, P. W. Deelman, and J. R. Petta, Science **355**, 156 (2016).
[48] A. Stockklauser, P. Scarlino, J. V. Koski, S. Gasparinetti, C. K. Andersen, C. Reichl, W. Wegscheider, T. Ihn, K. Ensslin, and A. Wallraff, Phys. Rev. X **7**, 011030 (2017).
[49] X. Mi, M. Benito, S. Putz, D. M. Zajac, J. M. Taylor, G. Burkard, and J. R. Petta, Nature (London) **555**, 599 EP (2018).
[50] N. Samkharadze, G. Zheng, N. Kalhor, D. Brousse, A. Sammak, U. C. Mendes, A. Blais, G. Scappucci, and L. M. K. Vandersypen, Science **359**, 1123 (2018).
[51] C. H. Yang, W. H. Lim, N. S. Lai, A. Rossi, A. Morello, and A. S. Dzurak, Phys. Rev. B **86**, 115319 (2012).
[52] D. M. Zajac, T. M. Hazard, X. Mi, E. Nielsen, and J. R. Petta, Phys. Rev. Applied **6**, 054013 (2016).
[53] X. Mi, C. G. Péterfalvi, G. Burkard, and J. R. Petta, Phys. Rev. Lett. **119**, 176803 (2017).
[54] D. A. Lidar, "Review of decoherence-free subspaces, noiseless subsystems, and dynamical decoupling," in *Quantum Information and Computation for Chemistry* (John Wiley & Sons, Inc., 2014) pp. 295–354.
[55] See Supplemental Material at [URL] for a detailed description of the theoretical model, the derivation of the effective Hamiltonian using a molecular orbital study, supporting numerical simulations, and additional information for the cavity-mediated two-qubit interaction. Refs. [68-90] appear in the supplement.
[56] J. R. Petta, A. C. Johnson, J. M. Taylor, E. A. Laird, A. Yacoby, M. D. Lukin, C. M. Marcus, M. P. Hanson, and A. C. Gossard, Science **309**, 2180 (2005).
[57] M. Atatüre, J. Dreiser, A. Badolato, A. Högele, K. Karrai, and A. Imamoglu, Science **312**, 551 (2006).
[58] V. Srinivasa, H. Xu, and J. M. Taylor, Phys. Rev. Lett. **114**, 226803 (2015).
[59] R. Hanson and G. Burkard, Phys. Rev. Lett. **98**, 050502 (2007).
[60] B. Bertrand, H. Flentje, S. Takada, M. Yamamoto, S. Tarucha, A. Ludwig, A. D. Wieck, C. Bäuerle, and T. Meunier, Phys. Rev. Lett. **115**, 096801 (2015).
[61] W. G. van der Wiel, S. De Franceschi, J. M. Elzerman, T. Fujisawa, S. Tarucha, and L. P. Kouwenhoven, Rev. Mod. Phys. **75**, 1 (2002).
[62] D. Bacon, arXiv:0305025.
[63] R. Woodworth, A. Mizel, and D. A. Lidar, J. Phys. Condens. Matter **18**, S721 (2006).
[64] F. Reiter, M. J. Kastoryano, and A. S. Sørensen, New J. Phys. **14**, 053022 (2012).
[65] J. I. Cirac and P. Zoller, Phys. Rev. Lett. **74**, 4091 (1995).
[66] N. Samkharadze, A. Bruno, P. Scarlino, G. Zheng, D. P. DiVincenzo, L. DiCarlo, and L. M. K. Vandersypen, Phys. Rev. Applied **5**, 044004 (2016).
[67] A. Pal, E. I. Rashba, and B. I. Halperin, Phys. Rev. X **4**, 011012 (2014).
[68] A. Auerbach, *Interacting Electrons and Quantum Magnetism (Graduate Texts in Contemporary Physics)* (Springer-Verlag Berlin and Heidelberg GmbH, 1998).
[69] G. Burkard and J. R. Petta, Phys. Rev. B **94**, 195305 (2016).
[70] D. A. Lidar, I. L. Chuang, and K. B. Whaley, Phys. Rev. Lett. **81**, 2594 (1998).
[71] G. Burkard, D. Loss, and D. P. DiVincenzo, Phys. Rev. B **59**, 2070 (1999).
[72] A. L. Saraiva, M. J. Calderón, X. Hu, S. Das Sarma, and B. Koiller, Phys. Rev. B **80**, 081305 (2009).
[73] D. Culcer, L. Cywiński, Q. Li, X. Hu, and S. Das Sarma, Phys. Rev. B **80**, 205302 (2009).
[74] X. Hu, Phys. Rev. B **83**, 165322 (2011).
[75] A. L. Saraiva, M. J. Calderón, R. B. Capaz, X. Hu, S. Das Sarma, and B. Koiller, Phys. Rev. B **84**, 155320 (2011).
[76] J. K. Gamble, M. Friesen, S. N. Coppersmith, and X. Hu, Phys. Rev. B **86**, 035302 (2012).
[77] Y. Wu and D. Culcer, Phys. Rev. B **86**, 035321 (2012).
[78] N. M. Zimmerman, P. Huang, and D. Culcer, Nano Lett. **17**, 4461 (2017).
[79] M. Friesen, S. Chutia, C. Tahan, and S. N. Coppersmith, Phys. Rev. B **75**, 115318 (2007).
[80] M. Friesen and S. N. Coppersmith, Phys. Rev. B **81**, 115324 (2010).
[81] D. Culcer, L. Cywiński, Q. Li, X. Hu, and S. Das Sarma, Phys. Rev. B **82**, 155312 (2010).
[82] D. Culcer, X. Hu, and S. Das Sarma, Phys. Rev. B **82**, 205315 (2010).
[83] C. Tahan and R. Joynt, Phys. Rev. B **89**, 075302 (2014).
[84] M. J. Rančić and G. Burkard, Phys. Rev. B **93**, 205433 (2016).
[85] N. Marzari, A. A. Mostofi, J. R. Yates, I. Souza, and D. Vanderbilt, Rev. Mod. Phys. **84**, 1419 (2012).
[86] E. Barnes, J. P. Kestner, N. T. T. Nguyen, and S. Das Sarma, Phys. Rev. B **84**, 235309 (2011).
[87] R. N. Annavarapu, American Journal of Computational and Applied Mathematics **3**, 33 (2013).
[88] S. Goswami, K. A. Slinker, M. Friesen, L. M. McGuire, J. L. Truitt, C. Tahan, L. J. Klein, J. O. Chu, P. M. Mooney, D. W. van der Weide, R. Joynt, S. N. Coppersmith, and M. A. Eriksson, Nature Physics **3**, 41 (2006).
[89] Z. Shi, C. B. Simmons, J. R. Prance, J. King Gamble, M. Friesen, D. E. Savage, M. G. Lagally, S. N. Coppersmith, and M. A. Eriksson, Applied Physics Letters **99**, 233108 (2011).
[90] L. Zhang, J.-W. Luo, A. Saraiva, B. Koiller, and A. Zunger, Nat. Commun. **4** (2013).